Effect of Hydrostatic Pressure on Optical Absorption Coefficient of InGaN/GaN of Multiple Quantum Well Solar Cells

Rajab Yahyazadeh[*,1], Zahra Hashempour[1]

[1] Department of Physics, Khoy branch, Islamic Azad University, Khoy, Iran

Abstract: In this paper, a numerical model is used to analyze an optical absorption coefficient according to the electronic properties of $InGaN/GaN$ multiple-quantum-well solar cells (MQWSC) under hydrostatic pressure. Finite difference techniques have been used to acquire energy eigenvalues and their corresponding eigenfunctions of $InGaN/GaN$ MQWSC and the hole eigenstates are calculated via a 6×6 k.p method under the applied hydrostatic pressure. All symmetry-allowed transitions up to the fifth subband of the quantum wells (multi-subband model) and barrier optical absorption, as well as the linewidth due to the carrier-carrier and carrier-longitudinal optical (LO) phonon scattering, are considered here. A change in the pressure up to 10 GPa increases the intraband scattering time up to 38fs and 40fs for light and heavy holes, respectively, raises the height of the Lorentz function and reduces the excitonic binding energy. The multi-subband model has a positive effect on the optical absorption coefficient and increases it by %17, contrary to the pressure function.

1. INTRODUCTION

Recently, indium gallium nitride alloys have attracted much attention for optoelectronic applications [1–4] due to their tunable energy bandgap varying from 0.7 eV to 3.4 eV [5-6]. The absorption range covers a significant portion of the solar spectrum, making InGaN a promising candidate for multi-junction solar cell systems. Moreover, with high radiation resistance, thermal stability, and chemical tolerance, InGaN solar cells could operate in extreme conditions [7]. The temperature and polarization dependence are considered preeminent tools in evaluating optical and electronic characteristics in III-V nanodevices

---

* Corresponding author. Email: **Rajab.yahyazadeh@iaukoy.ac.ir**

(e.g., solar cells and transistors) [8-11]. The optical absorption coefficients are one of the significant parameters in calculating recombination rate in InGaN/GaN Multi-quantum solar cell. Therefore, to study the recombination rate in detail, we must calculate the absorption coefficients in InGaN/GaN MQWSC. The effect of alloy on InGaN/GaN MQWSC has been investigated by Deng et al. [12]. Also, the temperature effect on InGaN/GaN MQWSC has been studied by Belghouthi et al. [13], and its efficiency in different wells and temperatures has been considered by Chouchen et al. [14]. In all these studies, a simple analytical relation of quantum well absorption coefficient has been used to obtain the electrical and electronic characteristic. Also, in our previous work [15], the absorption coefficient of quantum wells has been calculated for the first subband transition without considering other subbands. Further, we have not considered the effect of multi-subband, and the linewidth due to the carrier-carrier and carrier-longitudinal optical (LO) phonon scattering under external disturbances. This paper aims to perform these corrections under an external perturbation (e.g., hydrostatic pressure). In solar cells with a single-quantum well in the intrinsic region, due to the low absorption coefficient of second-and higher-order subbands, these energy transitions are not very effective in the recombination rate; however, in multi-quantum wells in the intrinsic region, the second-and higher-order transitions significantly affect the optical absorption due to more quantum wells. The linewidth function (Lorentz function) is one of the most important functions for calculating optical parameters, such as optical absorption coefficient and gain. The Lorentz function also depends on the scattering time and the transition energies. In all the work done on solar cells, this transition time under external perturbations is fixed and often considered to be 0.1ps; in the present study, we examine its dependence on pressure. The most important advantage of this numerical method and the aspect of innovation in this work is the use of five important parameters, including effective mass, energy gap, lattice constants, dielectric constant, quantum barrier, and well thickness, all of which are simultaneously dependent on hydrostatic pressure and temperature and have an analytical relation. We also consider the effect of hydrostatic pressure on the energy of heavy and light holes and the transition energy of the subbands. In this numerical model, the conduction band energy, wave functions, and energy subbands are obtained from the self-consistent solution of the Schrodinger and Poisson equations. The hole valance bands (heavy and light hole) energy, wave functions, and energy subbands are calculated using a 6×6 k.p method. The sample used in the modelling is the p–i–n solar cells with an InGaN/GaN MQWSC structure within the i-region. The p and n regions are based on GaN. The donor and acceptor concentrations in the n- and p-region materials are assumed to be the same as $0.1 \times 10^{18} \, cm^{-3}$, and 10 wells are considered in the current work. It should be notified that the calculated built-in polarization field for the structures is about $\sim 10^{8} \, Vm^{-1}$. In the present

research, atmospheric and hydrostatic pressures are taken into account, i.e., at zero hydrostatic pressure, only atmospheric pressure is applied. The results and discussions are obtained by calculating and drawing the figures.

2. CALCULATION MODEL

The quantum well solar cell (QWSC) consists of a multiple quantum well structure in the intrinsic region of a p–i–n. The MQW structure introduced for the model is constructed by a $In_mGa_{1-m}N$ with lower indium molar fraction (m=0.5) for wells and m=0.4 for barriers, as shown in Fig. 1. To obtain accurate values for Fermi energy, the energies of quantized levels within the two-dimensional electron gas (2DEG), potential profiles, wave function, and the sheet carrier concentration for the 2DEG in InGaN/GaN heterostructures, both the Schrodinger and Poisson equations must be solved. This is achieved by solving Schrodinger's equation and simultaneously taking into account the electrostatic potential obtained from Poisson's equation, as well as the image and exchange-correlation potentials using the three-point finite difference method [16]. In the Schrodinger equation, $eF_z z$ is the potential energy induced by the polarization charges, and F_z is the electric fields in the well (F_w) and barrier (F_b) caused by the spontaneous (SP) and piezoelectric (PZ) polarization [17-19]. In this work, five parameters, including effective mass, energy gap, lattice constants, dielectric constant and quantum barrier, and well thickness, are used, which are simultaneously dependent on hydrostatic pressure and temperature and have an analytical relation. The basal strain $\epsilon(T,P,m)=(a_s-a_e(T,P,m))/a_e(T,P,m)$ is expressed from the lattice of the substrate a_s and the epilayer $a_e(T,P,m)=a_0(m)\left[\left(1+\beta\left(T-T_{ref}\right)\right)\left(1-P/3B_0\right)\right]$. The lattice constants, as a function of temperature, indium molar fraction and the hydrostatic pressure[20-22], where $B_0=239GPa$ is the bulk modulus of sapphire. $\beta_{GaN}=5.56\times10^{-6}K^{-1}$ is the thermal expansion coefficient and $T_{ref}=300K$. $a_0(m)=0.13989m+0.03862$, is the equilibrium lattice constant as a function of indium molar fraction [21,22]. Here the dielectric constant and the thickness of InGaN, GaN depends on the hydrostatic pressure and temperature [20]. The band gap energy of InGaN/GaN is as following [17, 20, and 22]:

$$E_g(T,P)=E_g(0,0)+\gamma P+\sigma P^2+\left(\alpha T^2\right)/\left(T+T_e\right) \tag{1}$$

$E_g(0,0)$, stands for the band gap energy of GaN or InGaN in the absence of the hydrostatic pressure and at a temperature 0K. The suggested parameters used in Eq. (5) in our calculations have been taken from Ref 26. In this work,

parameters α, σ, γ etc. are independent of electron concentration. In the Schrödinger equation electron effective mass m^* can be written as[23]:

$$\frac{m_0}{m_e^*(P,T,m)} = 1 + \frac{E_P^\Gamma \left(E_g^\Gamma (P,T,m) + 2\Delta_{S0}/3 \right)}{E_g^\Gamma \left(E_g^\Gamma (P,T,m) + \Delta_{S0} \right)} \tag{2}$$

where m_0 is the free electron mass, E_P^Γ is the energy linked to the momentum matrix element, Δ_{S0} is the spin-orbit splitting, and $E_g^\Gamma (P,T,m)$ is the band gap variation as a function of the hydrostatic pressure and temperature. The hole wave functions and energy subbands are calculated along the Z-axis using a 6×6 k.p method [24,25]:

The optical absorption expression as a function of the photon energy E' is calculated as [26-29]:

$$\alpha_W (E') = \frac{\pi \hbar q^2}{E' \varepsilon_0 m_0^2 c n_{eff}} \times \sum_{i,j} \int_{E_{g,w}}^{E_{g,b}} D_{r,ij}^{2D} |Mij|^2 \left(f_{i_v} - f_{j_c} \right) L\left(E' - E_{ij} \right) dE_{ij} \tag{3}$$

where q and c are the electron charge and light vacuum speed; i and j are conduction and valance subband number respectively. $L\left(E' - E_{ij} \right) = \left(\Gamma_{hom}^2 \right) / 2\pi \left[\left(E' - E_{ij} \right)^2 + \Gamma_{hom}^2 \right]$ is the Lorentzian function, $D_r^{2D} = m_{r,ij} / \left(\pi \hbar^2 W \right)$ is the reduced density of allowed transition of each subband and $\left| M_{ij} \right|^2$ is the transition strengths. These three parameters are important in optical absorption. The Lorentz function depends on parameters Γ_{hom} and E_{ij}, which Γ_{hom} represent the linewidth of the conduction and the valance bands and is related to all scattering of carriers (electrons, light and heavy holes) and phonons (see Appendix A) [30,31]. The intraband relaxation time τ_{in} is obtained from Eqs. (A1) and (A4) as $\hbar / \tau_{in} = \Gamma_{cjk_\parallel}(E) + \Gamma_{vjk_\parallel}(E)$. Another effective parameter in the Lorentz function is $E_{ij} = E_i^e + E_j^h + E_g^{GaN} - E_b^{ij} - eF_W L_W$ [30]. That is the transition energy of the electron from the conduction band to the valance band. where E_i^e and E_j^h are the subband energy of electron and holes in triangular quantum well, respectively, E_b^{ij} is the bounding energy of excitons, Which is dependent on external perturbation such as pressure and temperature through electron and hole effective masses [32-33]. Exciton energies are determined employing a variational procedure [35]. Restricting ourselves to the

analysis of s-like excitons, this implies the proposal of a normalized trial wavefunction $|\Psi_x\rangle$, built from the product of uncorrelated electron and hole subband states together with the inclusion of a hydrogenic-s-like factor [34- 36]. Then, the exciton energy is obtained minimizing the functional $E_x = \langle \Psi_x | H_x | \Psi_x \rangle / \langle \Psi_x | \Psi_x \rangle$. where $H_x = H_e + H_{hh,lh} + H_\perp$ is the exciton Hamiltonian that includes the electron one-band Hamiltonian from the Schrodinger equation (H_e), the heavy and light hole six-band Hamiltonian from the K.P model where E_{i_c} and E_{j_v} are the quantized electron and hole energy levels, respectively $(H_{hh,lh})$, and the electron-hole interaction Hamiltonian $(H_\perp)$ [35-38]. The binding energy of the s-like exciton resulting from the coupling of the electron in the i-th subband and the hole in the j-th subband is then given by $E_b^{ij} = E_i^e + E_j^h - E_x$ [35]. The carrier effective mass in the i-th sub band can be calculated as follows [39,30]

$$\frac{1}{m_i^*} = \frac{1}{m_b^*}\left[1 - P_{iw}\right] + \frac{1}{m_w^*} P_{iw} \tag{4}$$

where m_b^* and m_w^* are the barrier and well carrier effective masses, $P_{iw} = P_{iw}(\psi_{iw})/\left(P_{ib}(\psi_{ib}) + P_{iw}(\psi_{iw})\right)$ is the probability of finding electron in the quantum well at the level with energy E_i .Which $P_{iw}(\psi_{iw}) = \int_0^{d_{GaN}} dz |\psi_{iw}|^2$ and $P_{ib}(\psi_{ib}) = \int_{-d_{InGaN}}^{0} dz |\psi_{ib}|^2$ are the wave function of the electron in the i-th subband and the wave function penetrating towards the quantum barrier , respectively. The value of the penetrating wave function in the barrier $(P_{ib}(\psi_{ib}))$, is the criterion for calculating the quantum confinement that is effective on the effective masses of the carriers in subbands . The effective masses of light and heavy holes are obtained using 6×6 k.p method [40]. The numerical values of the valance band effective mass parameters (Ai) and deformation potentials (Di) from reference 22 have been used. By determining the effective masses of carriers in quantum wells, through ternary formula $1/m_{In_xGa_{1-x}N}^* = \left((1-x)/m_{InN}^*\right) + x/m_{GaN}^*$, the effective masses in $m_{In_xGa_{1-x}N}^*$ barriers can be obtained [39]. By determining the effective mass of the electron in the i-th conduction subband and the effective mass of the hole in the j-th valance subband, the reduced effective mass $m_{r,ij}^{*-1} = m_i^{-1} + m_j^{-1}$ can be calculated. As a result, the reduced density of allowed transition of each subband (D_r^{2D}) can be calculated so that W is the thickness of the quantum well.

The transition matrix element $|M|^2$ is a measure for the strength of stimulated electron transitions in a given material. This strength does not depend on the direction of the intraband transition; it is the same for emission and absorption. However, the transition strength does depend on the angle between the electron wave vector $\vec{k}$ and the optical field vector $\vec{E}$. Any polarization direction of the optical field encounters a variety of electron $\vec{k}$ vectors that needs to be averaged at the given photon energy. For bulk zinc blende semiconductors, averaging over all possible $\vec{k}$ vectors results in an isotropic transition matrix element that is equal to the momentum matrix element ($M_b = (m_0 E_P)/6$) [27]. E_p, is the energy parameter whose numerical value is given in Table One. For quantum well structures, the transition matrix element is anisotropic and the absorption coefficient depends on the optical polarization. Commonly, one distinguishes two polarization modes, in which either the electric field (TE mode) or the magnetic field (TM mode) lies within the quantum well *xy*-plane (transversal plane). The compression strain increases the mean band gap and splits the degeneracy of the valence band maximum and introduces an anisotropic valence band structure. Note that the highest band is now heavy along $k_\perp$, the strain axis (growth direction) but light hole along $k_\parallel$. Consequently, the light beam has TE mode. The transition strengths of TE mode are different for heavy (hh) and light holes (lh) Which are calculated as the following relations [27, 42]

$$\left|M_{e-hh}^{TE}\right|^2 = \left(3 + 3\cos^2(\theta_e)\right) C_{ij} \left|M_b^2\right|/4 \qquad (5)$$

$$\left|M_{e-lh}^{TE}\right|^2 = \left(5 - 3\cos^2(\theta_e)\right) C_{ij} \left|M_b^2\right|/4 \qquad (6)$$

where $\cos(\theta_e) = E_{ij}/E'$ is the angular factor. $C_{ij} = \int \psi_i^*(x)\psi_j(x)dx$ is the electron-hole overlap integral. For TM Mode, the relationships are similar to 5 and 6, except that the inside of the parentheses in Equation 8 is $1 + 3\cos^2(\theta_e)$ (for heavy holes) and $1 + 3\cos^2(\theta_e)$ (for light holes). It should be noted that due to the finiteness of the quantum barriers, the orthogonal condition in the overlap integral as well as selection rule (i=j) no longer imposed and all symmetry-allowed transition are considered. $f_{i_c} = 1/1 + \exp\left(E_{i_c} - E_{f_c}\right)/k_b T$ and $f_{j_v} = 1/1 + \exp\left[\left(E_{j_v} - E_{f_v}\right)/k_b T\right]$ are the Fermi-Dirac distribution for electrons in i-th subband of conduction bands and holes in the j-th subband of valance bands, respectively. where E_{i_c} and E_{j_v} are the quantized electron and hole energy levels, respectively. E_{f_c} and E_{f_v} are the electron and hole quasi-Fermi level,

respectively. Finally, Adach's refractive index model for the $In_m Ga_{1-m}N$ is given by[27]

$$n_{eff} = \sqrt{A\left(\hbar\omega/E_g\right)^{-2}\left\{2 - \sqrt{1+\left(\hbar\omega/E_g\right)} - \sqrt{1+\left(\hbar\omega/E_g\right)}\right\} + B}\tag{7}$$

Here $A = 9.827(1-m) - 53.57m$ and $B = 2.736(1-m) - 9.19m$ are alloy-dependent parameters that are true for $m < 0.38$.

3. RESULTS AND DISCUSSION

In this paper, a numerical model is presented to calculate the optical parameters of $InGaN/GaN$ MQW Solar Cells (MQWSC), investigating the effect of hydrostatic pressure. Furthermore, Schrodinger and Poisson differential equations are solved by the finite difference method. However, the iterative method (mentioned in Refs. 43 and 45) is used in the step of the self-consistent solution of Schrodinger-Poisson equations. The convergence is obtained when the difference on the Fermi level associated with two consecutive iterations ($E_{F(n)} - E_{F(n-1)}$) is smaller than $10^{-4}eV$; during the calculations, the same grid mesh is also used for both Poisson and Schrödinger equations. The hole eigenstates are calculated along the Z-axis using a 6×6 k.p method. Figure 1 shows the dependence of the conduction band offset, the bandgaps of InGaN, and GaN on the hydrostatic pressure. The increase in the hydrostatic pressure with a range of 0-10Pa leads to increased conduction band offset. This is attributed to an increase in the bandgap energy of GaN and InGaN with increased hydrostatic pressure. This phenomenon is related to the correction of the atomic distances of the crystal lattice by external pressure, leading to a change in polarization. Conduction and valance bands with the location of quantum wells (electrons and holes), as well as valance bands for light and heavy holes, are shown in Figure 2. The optical absorption equation is proportional to the spatial overlap of electron-hole wave functions, $C_{ij,P}$ (P = 0, 5, 10), with 0 corresponding to the device under no pressure. The overlap under different pressures relative to $C_{ij,0}$ is extracted and plotted for the first and second subbands in Fig. 3. To explain the relationship between the quantum confinement and the overlap of electron and hole wave functions, one of the two-dimensional quantum wells was calculated and plotted with five subbands under the influence of different pressures according to Figure 4. In this figure, it is observed that the depth of the quantum well increases with increasing pressure. As a result, the greater the depth of the quantum well, the greater the quantum confinement of the carriers. In Figure 2, the electron waves functions of the first subband (which plays the most important role in the calculations due

to their high density) are plotted at different pressures. As shown in Figure 5, the height of the wave function increases by 2200 by increasing the pressure by 10 GPa, but its width decreases and it becomes closer to the interface of $GaN / In_{0.3}Ga_{0.7}N$, i.e. the expansion of the electronic wave function decreases in the GaN and $In_{0.3}Ga_{0.7}N$ regions. Similarly, the expansion of the hole wave function will also decrease by plotting the hole well. The lower the propagation of the wave function, the less their overlap. However, it should be noted that the amount of penetrating wave functions towards the quantum barriers must be calculated exactly in the effective mass reduced calculations. As shown in the inset, this amount of penetrating wave function decreases with increasing pressure. As a result, increasing the pressure increases the quantum confinement, reduces the penetrations of the wave function, and finally reduces the overlap of the electron and hole wave functions. The Lorentz function is one of the most influential parameters in the optical absorption equation and its shape. This function is examined in detail by calculating the pressure dependence of the conduction and valance linewidths, as illustrated in Figures 6 and 7, respectively. In particular, linewidths have a decreasing trend with increasing pressure. This is since the spatial separation of wave functions decreases with increasing the carrier density. In the case of scattering carriers with phonons (electron-phonon, heavy hole-phonon, and light hole-phonon), the decrease in linewidths is due to decreasing the term related to the Fermi function in the second term in the square bracket of Eq. (A4). The difference between the subband energy and the Fermi energy increases with increasing hydrostatic pressure, resulting in the decrease in the term related to the Fermi function. A reduction in the linewidths of the conduction and the valance bands increases the intraband relaxation time between the electrons and the light and heavy holes (Fig. 8) due to the inverse relationship of the intraband relaxation time with linewidths. According to this figure, an increase in the pressure by 10 GPa changes in the amount of intraband relaxation time to 38fs and 40fs for light and heavy holes, respectively. These changes are taken into account in the calculation of the Lorentz function. At zero pressure for heavy holes, intraband relaxation time value is equal to 0.097 picosecond (ps), approximately 0.1ps. In the calculations of other studies (mentioned in the introduction) this value is considered constant and equal to 0.1ps under changes such as barrier width, well width, various barrier alloys, and external perturbation. Transition energy is an effective parameter in calculating the Lorentz function, which also depends on the exciton binding energy and the subbands energy of the quantum wells. To better show the changes in these parameters, up to the second and third subbands are illustrated in Figures 9 and 10, respectively; however, symmetric-allowed transitions up to the fifth subband are entered in the calculations. It should be noted that the first and second subbands have the greatest effect (due to their high density). The binding energy of excitons as a

function of hydrostatic pressure is shown in Fig. 9. As seen in this figure, the decrease in the binding energy of excitons dependence with increasing pressure can be explained by the band offset and the internal electric fields. With increasing pressure, the spontaneous and piezoelectric polarization increases, thereby increasing the internal electric fields (F_w and F_b). The internal electric fields separate the electron and holes in the opposite direction, which reduces the overlap of electron and hole wave functions (Fig. 5), thus decreasing the binding energy of excitons. As the pressure increases, the band offset increases (Fig. 1), which expands the distance between the electrons and the holes, thus reducing the Coulomb interaction. It also increases the depth of quantum wells (Fig. 4), electron density, and quantum confinement, thus ultimately reducing the exciton binding energy. The transition energy of the carriers can be calculated by determining the energy of the subbands related to the carriers and the binding energy of excitons, as shown in Figure 10. According to the figure, the transition energies increase with increasing pressure. The Lorentz function for light and heavy holes of all symmetry-allowed transitions can be obtained by determining the transition energies and the linewidths of the carrier. For example, the plotted Lorentz function of the first subband transition (Fig. 11) corresponding to light and heavy holes indicates that the height of the Lorentz function increases while its width decreases with increasing pressure. They also shift to higher energies as the pressure increases up to 10, where the amount of increase in the Lorentz function height increases to 27 and 16 eV^{-1} for light and heavy holes, respectively. This increase, along with the decrease in width, is related to the decrease in linewidths, as illustrated in Figures 4 and 5. The Lorentz function transfer to high energies is also associated with the increase of transition energies with increasing pressure. By determining the Lorentz and the overlap function, as well as other parameters, the well absorption coefficient in terms of wavelength is plotted in Fig. 12. In this figure, the well absorption coefficients of other electronic transitions are less than E_{11} transitions; however, they are generally effective in the total absorption coefficient. Furthermore, the transitions with the greatest effect on the absorption coefficient are shown in this figure. The pressure effect on the absorption coefficient of quantum wells is illustrated in Figure 13, where the absorption coefficient decreases by increasing pressure, which is related to the increase in the energy gap. Heavy holes have more energy gaps than those of light holes thus they have less absorption. Consequently, the smaller peak corresponds to a heavy hole. In E_{11} transition, light holes also have low energy and therefore will have a larger wavelength than heavy holes. The second point is associated with changes in the amplitude of the absorption coefficient. As the pressure increases, the amplitude of the absorption coefficient decrees. The decrease in the amplitude of adsorption is related to the increase of quantum confinement with increasing pressure. The

stronger the quantum confinement, the lower the tendency to absorb energy. Therefore, increasing the pressure will decree the amplitude. An important result of the absorption coefficient is that the multi-subband model has a positive effect on the absorption coefficient and increases it by %17, contrary to the pressure function.

TABEL 1. Suggested Parameters for GaN and InN

| Parameters(unit)	GaN	InN	References
E_P^Γ(eV)	14.0	14.5	[21]
E_g^Γ(0K=0GPa)(eV)	3.42	0.7	[21]
Δ_{s0}(eV)	0.014	-0.001	[21]
γ(meV.GPa^{-1})	31.8	16	[19]
δ(meV.GPa^{-2})	-0.23	-0.02	[19]
S_{11}(10^{-2}GPa)	0.55	1.15	[16]
S_{12}(10^{-2}GPa)	0.19	0.46	[16]
α(10^{-3}eV.K^{-1})	0.909	0.245	[21]
T_e(K)	830	624	[21]
ε_∞	5.39	6.7	[45]
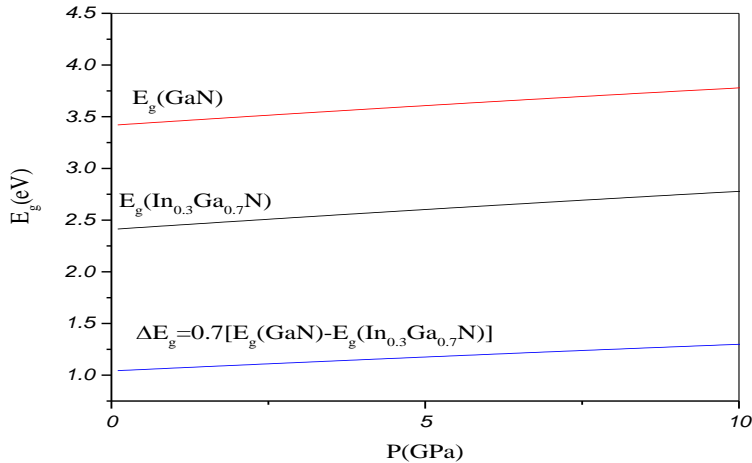
Fig. 1. Bandgaps energy of InGaN , GaN, and conduction band offset of InGaN/GaN MQW solar cell as a function of pressure.
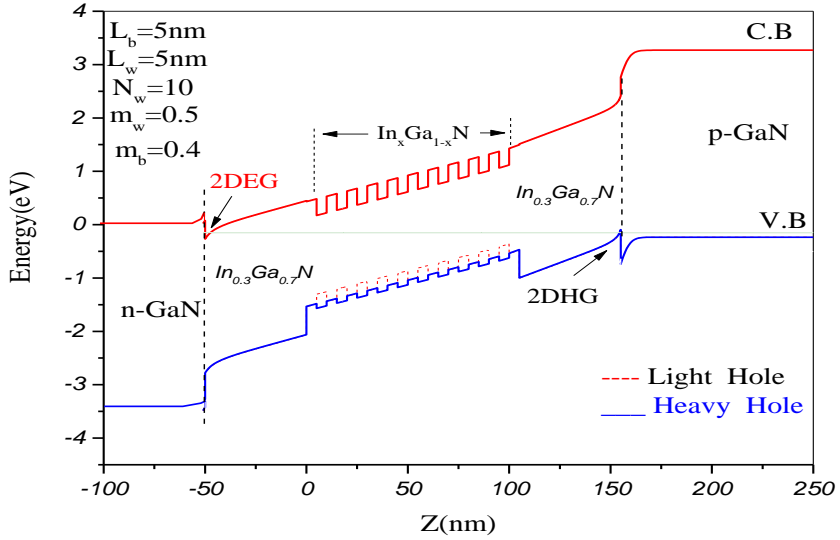
Fig. 2. The conduction (C.B) and valance (V.B) bands energy of InGaN/GaN MQW solar cell as a function of the distance under different hydrostatic pressure.
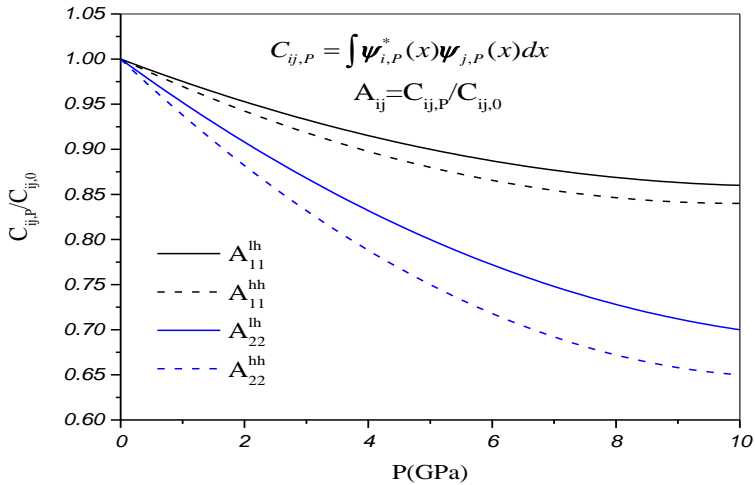

Fig. 3. Normalized overlap of the electron−hole wave functions versus hydrostatic pressure for InGaN/GaN MQW solar cell.
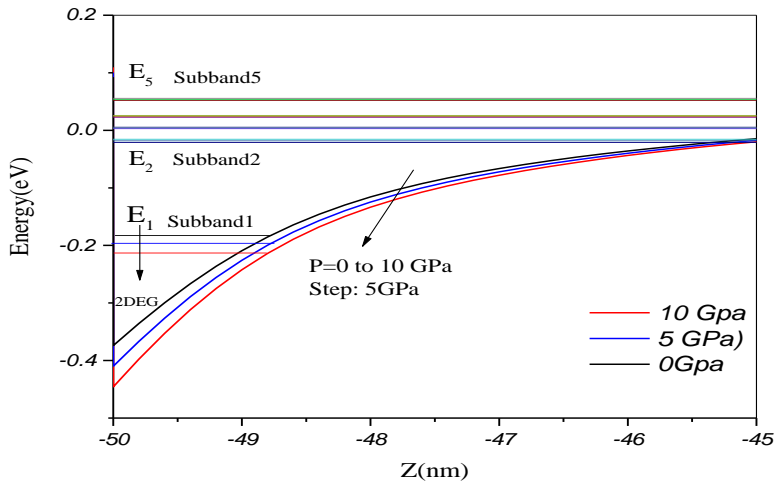
Fig. 4. The quantum well conduction band and subband of energy as a function of the distance under different hydrostatic pressures.
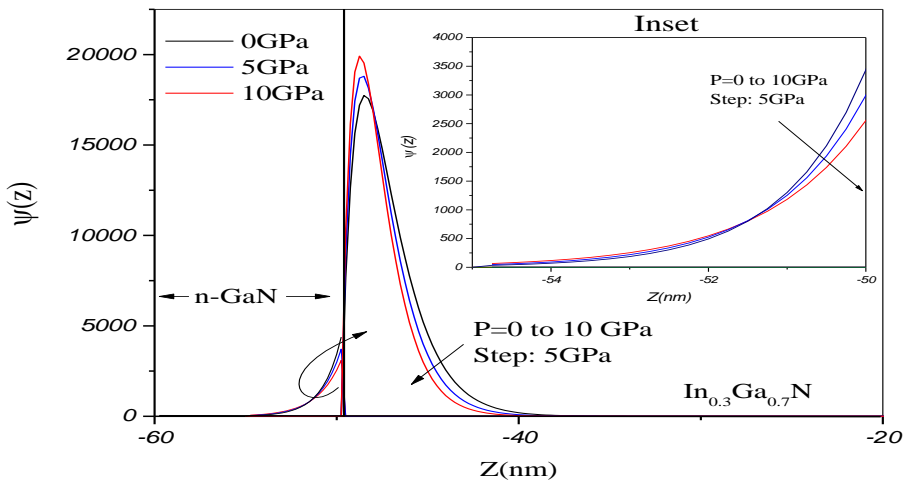

Fig. 5. The first subband electron waves function versus the distance for the $GaN / In_{0.3}Ga_{0.7}N$ MQW solar cell under different hydrostatic pressures. The inset indicates the electron wave function impenetrate to the GaN barrier.
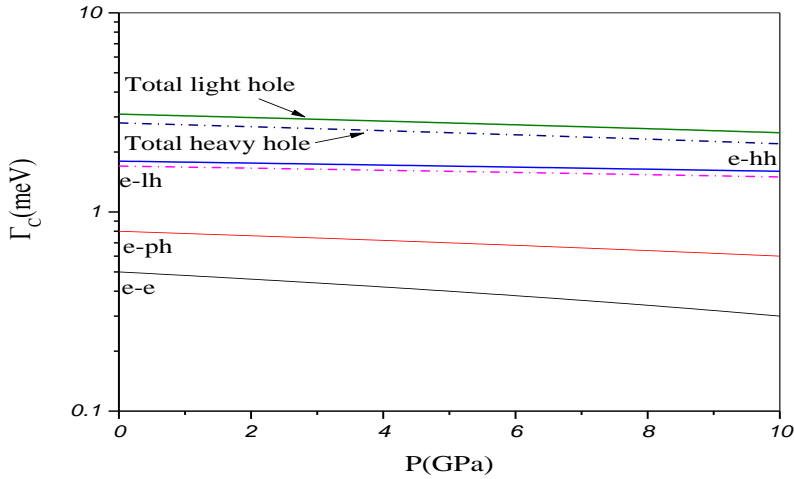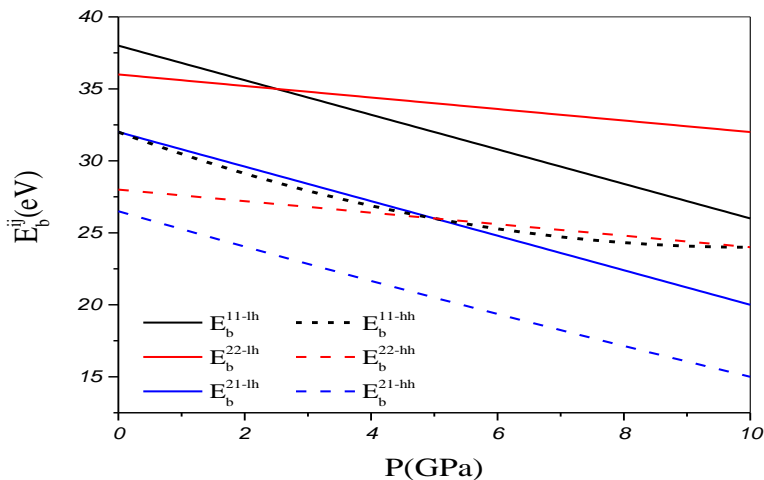
Fig. 6. Conduction band linewidths as a function of hydrostatic pressure at subband adage $\left(k_{\parallel} = 0\right)$ for *InGaN / GaN* MQW solar cell. In which all the scattering of electrons with other electrons(e-e), phonons(e-ph), light holes(e-lh) and heavy hole(e-hh) are considered.
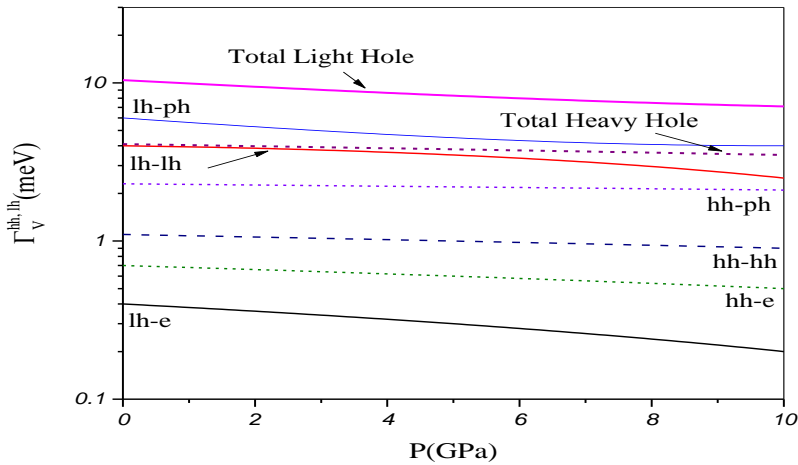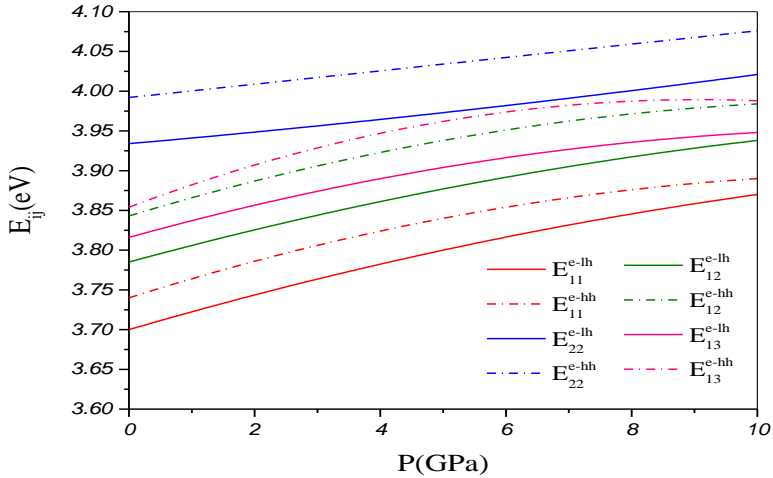

Fig. 7. Valance band linewidths as a function of hydrostatic pressure at subband adage $\left(k_{\parallel} = 0\right)$ for *InGaN / GaN* MQW solar cell. In which all the scattering of holes with other holes (hh-hh, lh-lh), phonons (lh-ph, hh-ph) and with other electrons (e-hh, e-lh) are considered.

.
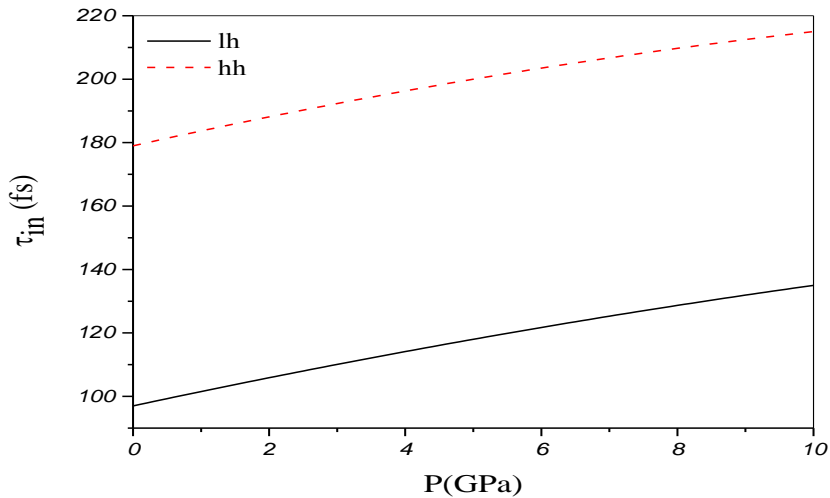
Fig. 8. Intraband relaxation time as a function of hydrostatic pressure at subband adage $\left(k_{\parallel} = 0\right)$ for *InGaN / GaN* MQW solar cell. In which heavy hole (solid line) and light hole (dashed line) are considered.


Fig. 9. Exciton Binding energy of heavy holes and light holes as a function of hydrostatic pressure for InGaN/GaN MQW solar cell.

Fig. 10. Transition energy as a function of hydrostatic pressure at subband adage $\left(k_{\|}=0\right)$ for $InGaN / GaN$ MQW solar cell. In which heavy hole (dashed line) and light hole (solid line) are considered.
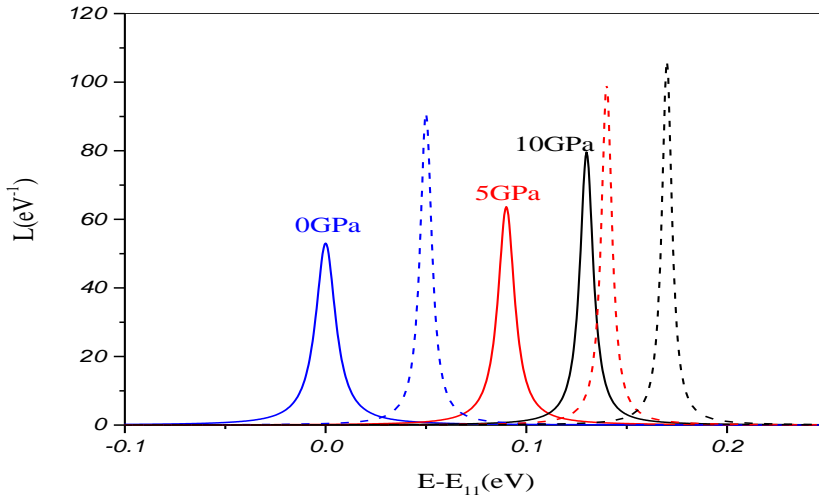
Fig. 11. Light hole (solid line) and heavy hole (dashed line) Lorentzian function versus of the energy difference $\left(E-E_{11}\right)$ under different hydrostatic pressures for $InGaN / GaN$ MQW solar cell, In which the energy transition between the first subbands of electron energy levels with holes are considered.
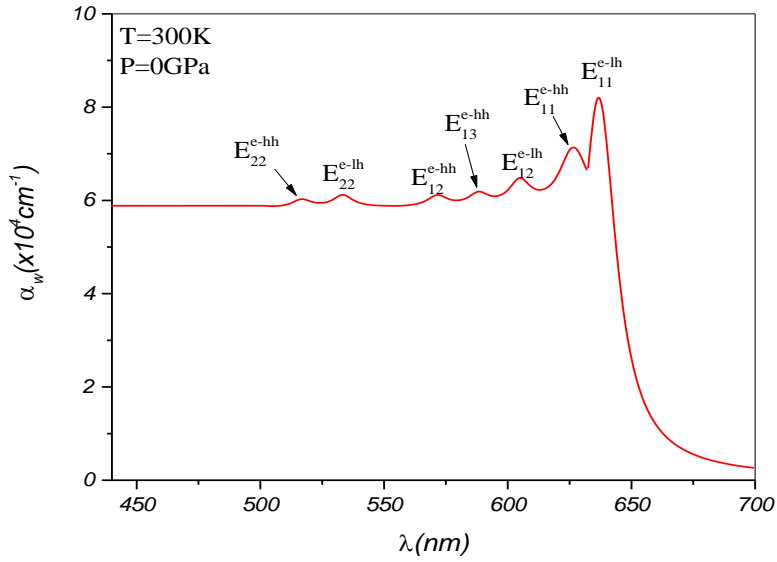
Fig. 12. Optical absorption versus wavelength for *InGaN / GaN* MQW solar cell.
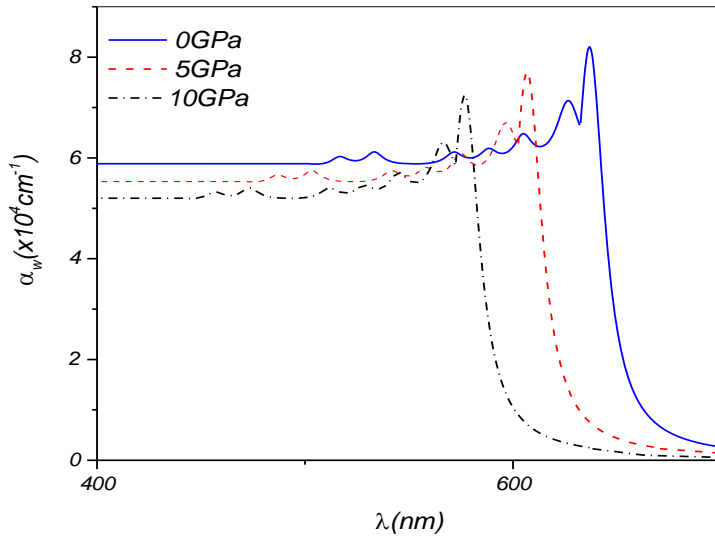
Fig. 13. Quantum well optical absorption versus wavelength under different hydrostatic pressures for *InGaN / GaN* MQW solar cell.

4. CONCLUSIONS

In this study, we examined the optical absorption spectrum, absorption coefficient, and radiative recombination rate of InGaN/GaN multi-quantum-well solar cells (MQWSC) under hydrostatic pressure. The results showed that increasing the hydrostatic pressure in the range of 0-10 GPa led to an increase in the amount of (I) the intraband relaxation time up to 38fs for heavy holes and 40fs for light holes and (II) the Lorentz function height to 27eV^{-1} for light holes and 17eV^{-1} for heavy holes, as well as a reduction in (III) the overlap of normalized wave functions and excitonic binding energy. The multi-subband model has a positive effect on the absorption coefficient and increases it by %17, contrary to the pressure function Therefore, it can be concluded that all effective transitions of quantum wells should be considered for an accurate study of absorption coefficient.

APPENDIX A: Intraband Relaxation Time

The linewidth due to the carrier-carrier scattering is obtained from the perturbation expansion of one-particle Green's functions. The linewidth for carrier-carrier scattering is given by:

$$\Gamma_{njk_{\|}}^{c-c} = \pi \sum_{n'=c,v} \sum_{k',p} \sum_{i,j} \left| V_{nm}(k_{\|}k_{\|}',ii',jj') \right| \times \delta\left(E + E_{n'ip_{\|}} - E_{nj'k_{\|}} - E_{n'i'p_{\|}'} \right)$$

(A1)

$$\times [f_n\left(E_{nj'k_{\|}}\right) f_{n'}\left(E_{n'i'p_{\|}'}\right) \left\{ 1 - f_{n'}\left(E_{n'ip_{\|}}\right)\right\} + \left\{ 1 - f_n\left(E_{nj'k_{\|}}\right)\right\} \left\{ 1 - f_{n'}\left(E_{n'ip_{\|}}\right)\right\} f_{n'}\left(E_{n'ip_{\|}}\right)$$

where n refers to conduction ($n = c$) or valence ($n = v$) bands, i, i', j, and j' are the subband numbers of the QW structure, and $f_n(E)$ is the Fermi distribution function. The interaction matrix element V_{nm} in a two-dimensional QW is given by

$$V_{nm}(k_{\|}k_{\|}',ii',jj') = \frac{e^2}{2\varepsilon_{GaN} A} \frac{\delta\left(k_{\|} - k_{\|}', p_{\|}' - p_{\|}\right)}{\sqrt{\left|k_{\|} - k'\right|^2 + \lambda_s^2}}$$

$$\times \iint \phi_{nj'}^*(z_1) \phi_{nj}(z_1) \phi_{ni'}^*(z_2) \phi_{n'i'}(z_1) \times \exp(-|z_1 - z_2| \sqrt{\left|k_{\|} - k'\right|^2 + \lambda_s^2}) dz_1 dz_2$$

(A2)

where the z-axis is perpendicular to the well interface, A is the interface area of the sample and the δ notation represents momentum conservation within a plane parallel to the well interface. $\phi_{nj}(z_1)$, is the wave function of a carrier, which is obtained by self-consistent solution of the Schrodinger-Poisson equation for electrons and k.p method for holes. λ_s, is the inverse screening length and its relation is as follows [33]

$$\lambda_s^2 = \frac{e^2}{\pi^2 \hbar^3 \varepsilon_{GaN}} \sum_j [m_{cj} f_c (E_{cj}) \sqrt{m_{cj} E_{cj}} + m_{vj} f_v (E_{vj}) \sqrt{m_{vj} E_{vj}}] \tag{A3}$$

Here m_{cj} and m_{vj} are the effective masses of electrons and holes in the conduction and valance bands, which will be explained in the following. For carrier-longitudinal optical (LO) phonon scattering, the linewidth broadening is obtained by taking the imaginary part of the one-phonon self-energy [34]

$$\Gamma_{njk_\parallel}^{c-ph} = \pi \sum_{k_\parallel'} \sum_{j'} \left| P_n (k_\parallel k_\parallel', jj') \right|^2 \times \tag{A4}$$

$$\times \left\{ n_q + 1 - f_n (E_{nj'k_\parallel}) \right\} \delta (E_{nj'k_\parallel'} - E + \hbar\omega_{LO}) + \left\{ n_q - f_n (E_{nj'k_\parallel}) \right\} \delta (E_{nj'k_\parallel'} - E - \hbar\omega_{LO})$$

where $\hbar\omega_{LO} = 91.13 meV^{-1}$ is the energy of the LO phonon and n_q is the phonon number per mode, given by $n_q = 1/\left[\exp(\beta\hbar\omega_{LO}) - 1 \right] \quad 1]$. The matrix element P_n for carrier-LO phonon scattering in a two-dimensional QW is given by

$$\left| P_n (k_\parallel k_\parallel', jj') \right|^2 = \sum_q \frac{e^2 \hbar\omega_{LO}}{2V} \left(\frac{1}{\varepsilon_\infty} - \frac{1}{\varepsilon} \right) \frac{q^2}{(q^2 + \lambda_s^2)} \times \left| \int \phi_{nj}^* (z) \phi_{nj} (z) \exp(-iq_z z) dz \right|^2 \tag{A5}$$

where ε_∞ is the optical dielectric constants, q_z is the phonon wave vector perpendicular to the well interface and V is the volume of the system. The intraband relaxation time τ_{in} is obtained from Eqs. (A1) and (A4) as $\hbar/\tau_{in} = \Gamma_{cjk_\parallel} (E) + \Gamma_{vjk_\parallel} (E)$.

REFERENCES

[1] C. Boudaoud, A. Hamdoune, Z. Allam. *Simulation and optimization of a tandem solar cell based on InGaN*. Mathematics and Computers in Simulation, 167 (2020) 194-201.

[2] M. Kuc, L. Piskorski, M. Dems, M. Wasiak, A. K. Sokoł, Robert P. Sarzała, T. Czyszanowski. *Numerical Investigation of the Impact of ITO, AlInN, Plasmonic GaN and Top Gold Metalization on Semipolar Green EELs*. Materials. 13 (2020) 1444.

[3] A. Tian, L. Hu, L. Zhang, J. Liu, H. Yang. *Design and growth of GaN-based blue and green laser diodes*. *Sci China Mate*. 63(8) (2020) 1348–1363.

[4] A. Pandey, W. J. Shin, J. Gim, R. Hovden, Z. Mi. *High-efficiency AlGaN/GaN/AlGaN tunnel junction ultraviolet light-emitting diodes*. Photonics Research. 8(3) (2020) 331-337.

[5] X. Huang, H. Chen et al. *Energy band engineering of InGaN/GaN multi-quantum-well solar cells via AlGaN electron- and hole-blocking layers*. Appl Phys Lett. 113(4) (2018) 043501.

[6] A.G. Bhuiyan, K. Sugita, A. Hashimoto, A. Yamamoto. *InGaN solar cells: present state of the art and important challenges*. IEEE J Photovolt. 2(3) (2012) 276-293.

[7] J. Wu, W. Walukiewicz et al. *Small band gap bowing in $In_{1-x}Ga_xN$ alloys*. Appl. Phys. Lett. 80 (2002) 4741.

[8] R. Yahyazadeh, *Effect of hydrostatic Pressure on Optical Absorption Spectrum AlGaN/GaN Multi-quantum wells*. Journal of Interfaces, Thin films, and Low dimensional systems. 3(2) (2021) 279-287.

[9] R. Yahyazadeh, Z. hashempour. *Effects of Hydrostatic Pressure and Temperature on the AlGaN/GaN High Electron Mobility Transistors*, Journal of Interfaces. Thin films, and Low dimensional systems. 2(2) (2019) 183-194.

[10] S. Z. H. Minabi, A. Keshavarz, A. Gharaati. *The effect of temperature on optical absorption cross section of bimetallic core-shell nano particles*. Journal of Optoelectronical Nanostructures. 1(3) (2016) 62-75.

[11] Y. Sefidgar, H. R. Saghai, H. G. K. Azar. *Enhancing Efficiency of Twobond Solar Cells Based on GaAs/InGaP*. Journal of Optoelectronical Nanostructures. 4(2) (2019) 84-102.

[12] Q. Deng et al. *An investigation on $In_xGa_{1-x}N$/GaN multiple quantum well solar cells*. J. Phy. D: Appl. Phy. 44 (2011) 265103.

[13] R. Belghouthi, M. Aillerie. *Temperatur dependece of InGaN/GaN Multiple quantum well solar cell*. Energy Procedia. 157 (2019) 793.

[14] B. Chouchen, M. H. Gazzah, A. Bajahzar, Hafedh Belmabrouk. *Numerical Modeling of the Electronic and Electrical Characteristics of InGaN/GaN-MQW Solar Cells*. Materials. 12 (2019) 1241.

[15] R. Yahyazadeh. *Numerical Modeling of the Electronic and Electrical Characteristics of InGaN/GaN Multiple Quantum Well Solar Cells*. J. of Photonics for Energy. 10 (2020) 045504.

[16] X. Huang. *Piezo-Phototronic Effect in a Quantum Well Structure*. ACS Nano. 10(5) 5145 (2016) 5145.

[17] O. Ambacher, A. B. Foutz, J. Smart, J. R. Shealy, N. G. Weimann, K. Chu et al. *Two dimensional electron gases induced by spontaneous and piezoelectric polarization in undoped and doped AlGaN/GaN heterostructures*. J. Appl. Phys. 87 (2000) 334.

[18] O. Ambacher, J. Majewski, C. Miskys, et al. *Pyroelectric properties of Al (In) GaN/GaN hetero- and quantum well structures*. J. Phys. Condens. Matter. 14 (2002) 3399.

[19] Z. J. Feng, Z. J. Cheng, and H. Yue. *Temperature dependence of Hall electron density of GaN-based heterostructures*. Chinese Physics. 13 (2004) 1334.

[20] V. Fiorentini, F. Bernardini, and O. Ambacher. *Evidence for nonlinear macroscopic polarization in III–V nitride alloy Heterostructures*. Appl. Phys. Lett. 80 (2002) 1204**.**

[21] P. Perlin, L. Mattos, N. A. Shapiro, J. Kruger, W. S. Wong, T. Sands, N. W. Cheung, E. R. Weber. *Reduction of the energy gap pressure coefficient of GaN due to the constraining presence of the sapphire substrate*. J. Appl. Phys. 85 (1999) 2385.

[22] K.J Bala, A. J Peter, C. W Lee. *Simultaneous effects of pressure and temperature on the optical transition energies in a Ga0.7In0.3N/GaN quantum ring*. Chemical Physics. 495 (2017) 42.

[23] I. Vurgaftman, J. R Meyer, L. R. R Mohan. *Band parameters for III–V compound semiconductors and their alloys*. J. Appl. Phys. 89 (2001) 5815.

[24] B. Jogai. *Influence of surface states on the two-dimensional electron gas in AlGaN/GaN heterojunction field-effect transistors*. Journal of Applied Physics. 93 (2003) 1631.

[25] B. Jogai. *Parasitic Hole Channels in AlGaN/GaN Heterojunction Structures*. Phys. stat. sol. (b). 233(3) (2002) 506.

[26] V. B. Yekta, H. Kaatuzian. *Design considerations to improve high temperature characteristics of 1.3μm AlGaInAs-InP uncooled multiple quantum well lasers: Strain in barriers*. Optik. 122 (2011) 514.

[27] J. Piprek, *Semiconductor Optoelectronic Devices: Introduction to Physics and Simulation*, Elsevier Scince, San Diego.California, 2013, 121-129.

[28] A. Horri, S. Z. Mirmoeini. *Analysis of Kirk Effect in Nanoscale Quantum Well Heterojunction Bipolar Transistor Laser*. Journal of Optoelectronical Nanostructures. 5(2) (2020) 25-38

[29] M. Cheraghizade. *Optoelectronic Properties of PbS Films: Effect of Carrier Gas*. Journal of Optoelectronical Nanostructures. 4(2) (2019) 1-12.

[30] P. S. Zory, *Quantum well lasers*, Academic. San Diego. Ca, 1993, 58-150.

[31] C.D. Mahan, *Many-body particle physics*, Plenum press, New York and London, 1990, 109-183.

[32] W. Wei-Ying et al. *Effects of interface roughness on photoluminescence full width at half maximum in GaN/AlGaN quantum wells*. Chin. Phys. B. 23(11) (2014) 117803.

[33] R. yahyazadeh, Z. Hashempour. *Numerical Modeling of Electronic and Electrical Characteristics of Multiple Quantum Well Solar Cells $Al_{0.3}Ga_{0.7}N$/GaN. Journal of Optoelectronical Nanostructures*. 5(3) (2020) 81.

[34] S. H. Ha, S. L. Ban. *Binding energies of excitons in a strained wurtzite GaN/AlGaN quantum well influenced by screening and hydrostatic pressure*. J. Phys.: Condens. Matter. 20 (2008) 085218.

[35] J.G. Rojas-Briseno, I. Rodriguez-Vargas, M. E. Mora-Ramos, J.C. Martínez-Orozco. *Heavy and light exciton states in c-AlGaN/GaN asymmetric double quantum wells*. Physica E. 124 (2020) 114248.

[36] P. Harrison, A. Valavanis, *Quantum Wells, Wires and Dots: Theoretical and Computational Physics of Semiconductor Nanostructures*, Wiley, 4th ed., 2016, 189-217.

[37] E. Kasapoglu, H. Sari, N. Balkan, I. Sokmen, Y. Ergun. *Binding energy of excitons in symmetric and asymmetric coupled double quantum wells in a uniform magnetic field*. Semicond. Sci. Technol. 15(2) (2000) 219.

[38] J.G. Rojas-Briseño, J.C. Martínez-Orozco, M.E. Mora-Ramos. *States of direct and indirect excitons in strained zinc-blende GaN/InGaN asymmetric quantum wells*. *Superlattices and Microstructures*. 112 (2017) 574-583.

[39] R Yahyazadeh*, Z.Hashempour. *Effect of Hydrostatic Pressure and Temperature on Quantum Confinement of AlGaN/GaN HEMTs*.   Journal of Science and Technology. 13(1) (2021) 1-11.

[40] S.L. Chung, C.S. Chang. *k.p method for strained wurtzite semiconductor*. Phys. Rev. B. 54 (1996) 2502.

[41] S. Adachi, *Physical Properties of III-V compounds*, John Wiley & Sons, 1992, 290.

[42] S. R. Chinn, P. S. Zory, A. R. Reisinger. *A Modal for Grin-SCH-SQW Diode Lasers*. IEEE Journal of quantum Electronics. 24(11) (1988) 2191.

[43] I. Tan, G. L. Snider, L. D. Chang, E. L. Hu. *A self-consistent solution of Schrödinger–Poisson equations using a nonuniform mesh*. J. Appl. Phys. 68 (1990) 4071.

[44] X. Huang et al. *Piezo-Phototronic Effect in a Quantum Well Structure*. ACS Nano. 10 (2016) 5145.

[45] Z. Dongmei, W. Zongchi, X. Boqi. *Correlated electron–hole transitions in wurtzite GaN quantum dots: the effects of strain and hydrostatic pressure*. J. Semicond. 33 (2012) 052002.